Title

Experimental and Computational Evidence of Highly Active Fe Impurity Sites on the Surface of Oxidized Au for the Electrocatalytic Oxidation of Water in Basic Media

Journal

ChemElectroChem, 3(1)

ISSN

2196-0216

Authors

Klaus, Shannon
Trotochaud, Lena
Cheng, Mu-Jeng
et al.

Publication Date

2016

DOI

10.1002/celc.201500364

Peer reviewed

Experimental and Computational Evidence of Highly-Active Fe Impurity Sites on the Surface of Oxidized Au for the Electrocatalytic Oxidation of Water in Basic Media

Shannon Klaus,[a][b]§ Lena Trotochaud,[a]§ Mu-Jeng Cheng,[a] §
Martin Head-Gordon[a][c], and Alexis T. Bell*[a][b]

[a]Joint Center for Artificial Photosynthesis, Lawrence Berkeley National Laboratory, Berkeley, California 94720, United States

[b]Department of Chemical and Biomolecular Engineering, University of California at Berkeley, Berkeley, California 94720, United States

[c]Department of Chemistry, University of California at Berkeley, Berkeley, California 94720, United States

Submitted to
ChemElectroChem
August 10, 2015

*Corresponding author email: bell@cchem.berkeley.edu

§These authors contributed equally.

Abstract

Addition of Fe to Ni- and Co-based (oxy)hydroxides significantly enhances the activity of these materials for electrochemical oxygen evolution reaction (OER). Here, we show that Fe cations bound to the surface of oxidized Au enhance its OER activity, the OER activity increasing with increasing surface concentration of Fe. Density functional theory analysis of the energetics of the OER revealed that oxygen evolution over Fe cations bound to a hydroxyl-terminated oxidized Au surface (Fe-Au_2O_3) occurs at an overpotential 0.43 V lower than that at which the OER occurs on hydroxylated Au_2O_3 (0.86 V). This finding agrees very well with experimental observation and is a consequence of the more optimal binding energetics for the OER reaction intermediates at Fe cations bound to the surface of Au_2O_3. These findings suggest that the enhanced OER activity reported recently upon low-potential cycling of Au may be due to surface Fe impurities rather than to “superactive” Au(III) surfaquo species.

1. Introduction

The development of highly active, earth-abundant catalysts for the oxygen evolution reaction (OER, in basic media: $4HO^- \rightarrow 2H_2O + O_2 + 4e^-$) is critical for achieving the efficient photoelectrochemical conversion of solar energy to chemical fuels.[1] A number of studies have shown that the incorporation of Fe into various (oxy)hydroxides can improve their OER activity dramatically.[1j, 2] Investigations of Ni-(oxy)hydroxides have shown that ppb-level Fe impurities in basic electrolytes enhance the activity of Ni-based catalysts by as much as 200 fold.[2b, 2c, 2k] Experimental and theoretical analysis of the OER on such $Ni_{1-x}Fe_xOOH$ materials indicate that the Fe cations substituted into the Ni-(oxy)hydroxide lattice are the active sites responsible for high catalytic activity.[2d] Similarly, recent work by Burke et al. has proposed that Fe substituted into Co-(oxy)hydroxides may be the catalytically active sites.[2a] This work has also noted that the low activity of Fe^{3+} cations in FeOOH could be due to the low conductivity of this material and that the enhanced activity upon Fe addition into CoOOH (or NiOOH) is the result of the active Fe^{3+} sites being contained in an appropriately conductive and chemically stable host structure.

Despite these experimental efforts, the precise role that Fe plays in improving the energetics of the reaction is still unclear, and a better understanding of the OER mechanism at these highly-active Fe-containing materials could enable the development of new catalysts with improved activity and/or stability (e.g., for use in acidic media). Density-functional theory (DFT) can provide mechanistic insight, but such efforts are often challenging. In the case of Ni-(oxy)hydroxides, recent work by Friebel et al. has found that Fe^{3+} cations within $Ni_{1-x}Fe_xOOH$ exhibit a significantly lower OER overpotential compared to Ni cations in either $Ni_{1-x}Fe_xOOH$ or pure NiOOH.[2d] It should be noted, though, that the theoretical simulation of Ni- and Co-(oxy)hydroxides is complex because these materials have highly disordered layered structures and are known to intercalate alkali cations, water, and hydroxide anions, making it difficult to define unambiguously the composition and structure of the host catalyst.

The work presented here is motivated by the recent observation by Trotochaud et al. that removal of Fe impurities from alkaline electrolyte results in a decrease in OER activity over Au.[2c] Subsequent work by Doyle and Lyons has proposed that “superactive” sites are formed on the surface of an Au electrode during low-potential cycling in unpurified NaOH.[3] The authors ascribed the increased activity to the formation of highly active hydrous monomeric Au(III)

surfaquo species. It should be noted, though, that studies reporting such activity improvement for Au were likely carried out using electrolytes containing Fe impurities.[3-4] It is also quite likely that Fe impurities in the electrolyte may have influenced other investigations of the oxygen evolution over Au in alkaline electrolytes.[5] It is well established that Au is oxidized at potentials relevant to the OER to Au(III) (either as $Au(OH)_3$ or Au_2O_3), and the structure of the surface oxide(s) formed is well-defined.[6] Therefore, the influence of Fe cations bound to the surface of Au_2O_3 is expected to be a simpler system for DFT analysis compared to Ni- and Co-(oxy)hydroxides.

Here, we report experimental and theoretical efforts aimed at identifying the role of Fe cations deposited onto the surface of Au oxide on the rate of oxygen evolution at low overpotentials (<0.4 V vs Hg/HgO). We confirm experimentally that in the presence of Fe electrolyte impurities, oxidized Au electrodes exhibit an enhancement in OER activity, which increases with increasing content of surface Fe. In contrast to Ni-(oxy)hydroxides, where Fe is incorporated throughout the (oxy)hydroxide structure,[2b, 2c, 2e] we show that Fe binds reversibly to the Au surface. Density functional theory analysis of the relative energies of OER reaction intermediates reveals that the overpotential for the OER onset on Fe^{3+} sites bound to the surface of Au_2O_3 is 0.4 V lower than that for Au^{3+} sites present on the surface of the host oxide, in very good agreement with the experimentally observed difference in overpotentials for Fe-containing and Fe-free Au_2O_3.

2. Experimental and Theoretical Methods

2.1. Electrode Preparation and Electrochemical Characterization

All electrochemical measurements were carried out in a Teflon PFA beaker (VWR 13917-582) to eliminate contamination due to glass etching from the alkaline electrolyte. A coiled Pt wire served as the counter electrode (99.95%, DOE Business Center for Precious Metals Sales and Recovery – BCPMSR) and was housed in a porous polypropylene compartment inside the electrochemical cell. Pt counter electrode wires were periodically cleaned by overnight soaking in 6 M nitric acid. Potentials were applied using a BioLogic SP-200 potentiostat and are reported vs the Hg/HgO reference electrode (CH Instruments) filled with 1 M KOH, for which the equilibrium potential for OER is 0.306 V (in 1 M KOH). The uncompensated series resistance R_u was determined by potentiostatic electrochemical impedance

spectroscopy prior to each voltammogram, and the measured R_u value was internally compensated at 95%.

Depending on the experiment, three types of KOH were utilized: “Fe-free”, “reagent-grade”, and “electronic-grade”. “Fe-free” 1 M KOH electrolyte was obtained by following the procedure of Trotochaud et al.[2c] (a full description is provided in the Supporting Information S1). “Reagent-grade” 1 M KOH was prepared using ACS reagent-grade KOH pellets (≥85%, ≤0.001% Fe, Sigma-Aldrich 221473), and “electronic-grade” 1 M KOH was prepared from Baker Analyzed Electronic Grade KOH solution (45%, <1.000 ppm Fe, VWR JT3144-3). Investigations of activity changes due to the presence of Fe impurities were completed using all three electrolytes.

Au rotating disc electrodes (RDEs, 5 mm diameter) were used for all electrochemical measurements and were fabricated using 99.95% purity Au (DOE BCPMSR). Prior to electrochemical measurements on bare Au, Au RDEs were mechanically polished with 1 and 0.05 mm alumina slurries, with 10 min of sonication in ultrapure water (18.2 MΩ cm, EMD Millipore) after each polishing step. The Au surface was then stabilized through 25 electrochemical cycles from -1.0 to 0.7 V vs Hg/HgO at 10 mV s^{-1} in 0.1 M “Fe-free” KOH. The electrodes were then rinsed briefly with ultrapure water and dried under a N_2 gas stream prior to electrochemical measurements.

2.2. Inductively Coupled Plasma Mass Spectrometry

The measurement of Fe, Ni, and Co content of catalyst films and KOH electrolyte solutions was carried out using an Elan DRC (Perkin Elmer) inductively coupled plasma mass spectrometer (ICP-MS) with a glass nebulizer (Micromist) and spray chamber at 1300W RF power. Ammonia was used as a reaction gas to remove plasma-based interferences for Fe analysis. Films were dissolved in 5 M high purity nitric acid (Sigma-Aldrich 84385) overnight and sonicated for 20 min prior to dilution. Final solutions for analysis contained ~2 wt% nitric acid. Prior to ICP-MS measurement, the KOH electrolytes were diluted ~10× with 2 wt% ultra-high purity nitric acid.

Electrolyte metal contents were calculated using 0-50 ppb calibration standards of Ni, Fe, and Co. Calibrations were confirmed by comparison to standard solutions of these elements. High purity KNO_3 (ICP-MS grade) was added to all standards to matrix-match the concentration of potassium ions present in these solutions to those estimated to be present within the 1 M KOH

electrolytes. The detection limit approached the lowest calibration standard and is estimated to be ~0.2 ppb. The most abundant isotopes of analytes were chosen for analysis (56, 60, and 59 for Fe, Ni and Co, respectively).

2.3. X-ray Photoelectron Spectroscopy

X-ray photoelectron spectra were collected with a Kratos Axis Ultra spectrometer using a non-monochromatic Mg Kα source (10 mA, 15 kV) to avoid any LMM Auger features from trace Ni overlapping with the Fe $2p_{3/2}$ region. The base pressure in the analytical chamber was $\sim 7\times10^{-9}$ Torr. Spectra were collected with 20 eV pass energy and 50 meV step size. The Fe 2p regions were collected using dwell times of 300-500 ms and are an average of 20 scans to obtain sufficient spectral signal-to-noise. The Au 4f spectrum (Au $4f_{7/2}$ at 84.0 eV)[7] was used for spectral charge-shift calibration. All spectra were analyzed using CasaXPS (Casa Software, Ltd).

2.4. Computational Details

Density functional theory (DFT) calculations were performed using the Vienna ab initio Simulation Package (VASP) with the projector augmented wave pseudopotentials and the PBE functional. The plane wave energy cutoff was set to 400 eV and the density cutoff was set to 700 eV, and electron smearing was employed using the Gaussian-smearing technique with a width of k_BT = 0.1 eV for the surfaces and 0.01 eV for molecules. All calculated values of energy were extrapolated to $k_BT = 0$.

For the surface calculations, at least 10 Å vacuum space between adjacent images was used to prevent the interaction between the replicas along the z-direction, while for all molecules, a 20 Å × 20 Å × 20 Å box was used for simulations. Spin-polarized wavefunctions were used for all calculations except H_2 and H_2O, in which non-spin-polarized wavefunctions were used. To convert electronic energies into Gibbs free energies, zero-point energy (ZPE), enthalpic, and entropic corrections, and solvation energies are needed. We used the numbers reported by Rossmeisl et al. for ZPE and thermodynamic corrections,[8] and the solvation corrections were calculated using the Poisson-Boltzmann implicit solvation model with a dielectric constant ε = 80 for water. The computational standard hydrogen electrode model proposed by Nørskov and co-workers[9] was used to calculate potential- and pH-dependent free energy surfaces. We emphasize that this is a purely thermodynamic study, which means no kinetic barriers are calculated or included in the Gibbs free energy surfaces. This simple thermodynamic analysis has been shown to satisfactorily predict experimental overpotentials for other electrocatalytic

reactions,[8, 10] and the thermodynamic overpotentials provided here represent the lower bounds to the kinetic ones. Moreover, recent computational studies have shown that the kinetic barriers are small and thus surmountable at room temperature.[11]

3. Results and Discussion

3.1. Electrochemical characterization of Au in KOH electrolytes with varying Fe impurity contents

The concentration of Fe, Ni, and Co impurities in each 1 M solution of KOH was determined using ICP-MS (Table 1). The "Fe-free" solution was prepared by following the method for removing Fe-impurities from KOH reported recently by Trotochaud et al.[2c] and contains Fe below the ICP-MS detection limit (estimated to be ~0.2 ppb for each metal). The reagent-grade 1 M solution of KOH also contains Fe below the detection limit. In contrast, the electronic-grade KOH solution contains ~76 ppb of Fe. We note that the Fe-free electrolyte is the purified version of the electronic-grade KOH.

The amount of Ni and Co in each electrolyte solution was measured to rule out the possibility that highly-active $Ni_{1-x}Fe_xOOH$ or $Co_{1-x}Fe_xOOH$ species predominate at the electrode surface; both elements were consistently below the ~0.2 ppb detection limit. However, we note that for a sample of Fe-free 1 M KOH collected immediately after the last purification step (centrifugation to remove the $Ni(OH)_2$), a high Ni concentration was detected (>400 ppb). This is in contrast to four other Fe-free samples collected >1 h after the final purification step, which contained Ni concentrations below ICP-MS detection. Although "Fe-free" solutions are centrifuged to remove $Ni(OH)_2$, this result suggests that some amount of $Ni(OH)_2$ remains in the purified KOH solution even after centrifugation. The decreased concentration of Ni detected by ICP-MS with a longer time elapsed after purification is due most likely to the slow settling of $Ni(OH)_2$ to the bottom of the bottle in which the solution was stored. For all electrochemical experiments reported here, Fe-free 1 M KOH was only used >1 h after purification.

Table 1. Metal contents of prepared 1 M KOH electrolyte solutions

	Fe concentration (ppb)	**Ni concentration** (ppb)	**Co concentration** (ppb)
Fe-free 1 M KOH	below detection	below detection*	below detection
Reagent-grade 1 M KOH	below detection	below detection	below detection
Electronic-grade 1 M KOH	76.4 ± 8.8	below detection	below detection

* All Fe-free 1 M KOH solutions measured >1 h after the last purification step contained Ni below the detection limit.

Table 1 demonstrates that the purification procedure used to remove Fe impurities from the electronic-grade KOH is effective. However, the presence of Ni impurities in the Fe-free electrolyte cannot be completely ruled out due to the use of $Ni(OH)_2$ during purification and its persistence after centrifugation. This raises the question of whether Ni impurities together with the Fe impurities affect the catalytic properties of the Au electrode. We show below that that any Ni impurities present have a negligible effect on the oxygen evolution activity.

The influence of varying the KOH electrolyte on the oxygen evolution current observed over Au is shown in Figure 1. A >200 mV decrease in the OER onset potential is observed in cyclic voltammograms (CVs) for Au electrodes in electronic-grade KOH, in which Fe impurities are present. These findings are consistent with those reported by Trotochaud et al., who noted that the removal of Fe from the electrolyte dramatically increased the overpotential required for OER on bare Au substrates.[2c] As shown in Figure S3, the OER current increases with systematic increases in the concentration of Fe impurities in the electrolyte. It is interesting to note that CVs over Au appear to be highly sensitive to the concentration of Fe present in the electrolyte, and can distinguish between small differences in Fe concentrations not discernable by ICP-MS (i.e., a difference in Fe-free vs reagent-grade KOH is clearly observed, even though ICP-MS analysis of both electrolytes gives Fe below the detection limit). For all electrolytes, rotation of the Au electrode further increases the measured OER current. Since these current densities are below those at which mass-transfer effects are typically observed, the effect of rotation is presumably due to exposure of the electrode to a larger total volume of electrolyte (i.e., accumulation of a larger quantity of Fe impurities at the electrode surface).

When the electrode is rotated at 1600 rpm in 1 M Fe-free KOH (used after >1 h after purification), small oxidation/reduction features associated with the conversion of $Ni(OH)_2$/NiOOH are observed. (As noted above, some amount of $Ni(OH)_2$ is present in the electrolyte as a consequence of the cleaning procedure used. For further information, see Supporting Information S2). For all other samples, only the surface oxidation/reduction of Au is observed at 0.35/0.20 V, and the positions and intensities of these features are unaffected by the level of Fe present in the electrolyte, indicating that the surface of the Au electrode remains electrochemically accessible and the energetics of the Au redox processes are minimally affected by Fe (or Ni) impurities.

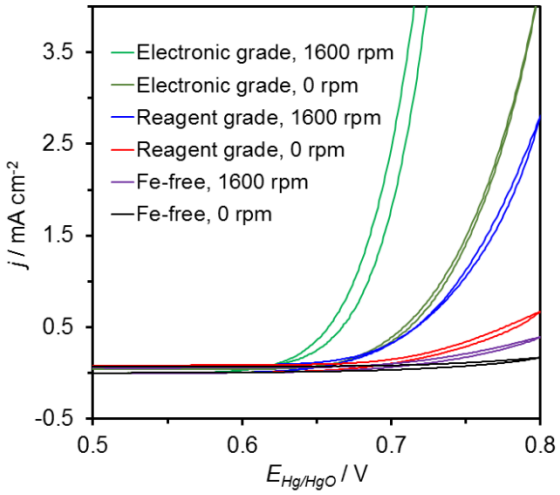

Figure 1. Cyclic voltammograms of Au cycled in 1 M KOH diluted from as-received stock solution or pellets (for electronic-grade and reagent-grade, respectively), or purified according to ref. [2c] (Fe-free). The potential scan rate was 10 mV s^{-1} between 0.0 and 0.8 V vs Hg/HgO, for which E^0 for the OER is 0.306 V.

Since Ni impurities are also present in the case of Fe-free KOH, and may be present in other electrolytes below the detection limit of ICP-MS, it is important to assess whether the observed increase in OER activity could also be affected by these low-level Ni impurities (or the combination of Fe and Ni, which is known to be highly-active for the OER). X-ray photoelectron spectra (XPS) were taken of Au electrodes at the end of a series of CV scans (Figure 2) in order to determine the degree of accumulation of Ni and Fe on the Au surface. An Fe XPS signal was not observed for the electrode cycled in purified ("Fe-free") 1 M KOH, confirming that this

electrolyte is effectively free of Fe. In contrast, low intensity features in the Fe 2p region can be seen for the Au electrodes cycled at both 0 rpm and 1600 rpm in reagent-grade KOH, consistent with the observed increase in OER current density for reagent-grade vs Fe-free KOH. The Au electrodes cycled with and without 1600 rpm rotation in electronic-grade KOH exhibit the greatest Fe 2p contributions, consistent with the much higher Fe concentration measured in this electrolyte (see Table 1). For both reagent-grade and electronic-grade KOH, rotation during the CV acquisition resulted in greater uptake of Fe on the Au surface and a coincident increase in the OER current. Surface accumulation of Ni was detected for all samples via XPS at very low levels (calculated to be between 1.6 and 3%), except for Au cycled in Fe-free 1 M KOH (> 1 h after purification) at 1600 rpm, which has a much larger Ni 2p contribution.

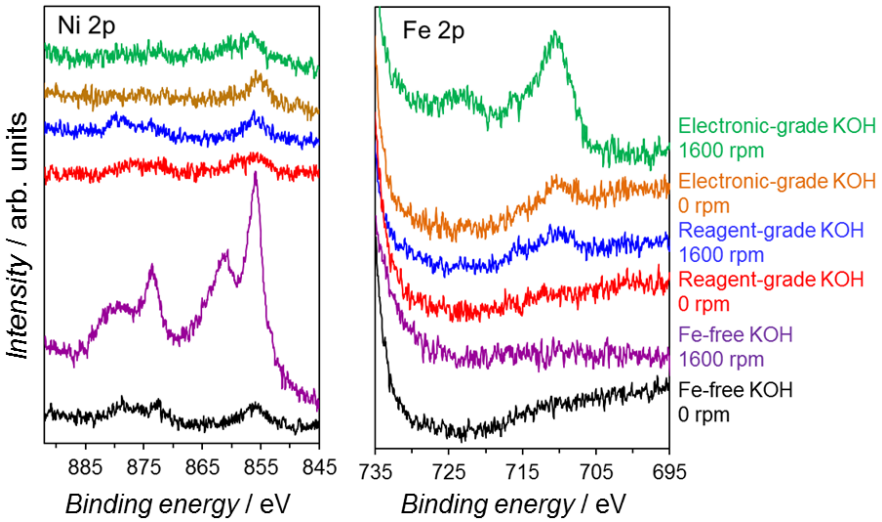

Figure 2. Ni 2p and Fe 2p photoelectron spectra of Au electrodes after 10 CV cycles (final cycle of which is shown in Figure 1) in Fe-free 1 M KOH at 0 and 1600 rpm (black and purple), reagent-grade 1 M KOH at 0 and 1600 rpm (red and blue), and electronic-grade 1 M KOH at 0 and 1600 rpm (orange and green). Raw data were smoothed using 3-point adjacent averaging.

The XPS data combined with our other experimental findings indicate that formation of a highly-active Fe-Ni (oxy)hydroxide is not the cause for the increased OER activity over Au for the following reasons:

1) $Ni_{1-x}Fe_x(OH)_2/Ni_{1-x}Fe_xOOH$ reduction/oxidation features were not observed in cyclic voltammograms for the samples where XPS showed only trace Ni at the electrode surface.
2) The surface coverage by Ni of these sample is small (less than ~3% of the Au surface contribution via XPS – see Table S1) and is nearly constant.
3) The increase in OER activity correlates with the surface concentration of Fe observed by XPS and ICP-MS.

Therefore, we conclude that while a small, nearly constant amount of Ni is present on the Au surface in all cases after CV cycling, the observed changes in oxygen evolution activity over Au correlate with the varying concentration of Fe in the electrolyte and the degree of Fe accumulation on the surface of the electrode. Hence, the changes in OER activity observed are attributed solely to changes in the presence of Fe on the electrode surface.

3.2 Reversibility of Fe adsorption over Au

Additional CV and XPS experiments were carried out with the aim of identifying whether the Fe impurities bind reversibly or irreversibly onto the Au surface. Au electrodes cycled in electronic-grade KOH show dramatic increases in OER activity, but when these same electrodes are subsequently transferred to “Fe-free” KOH and additional CV cycles are carried out, the OER current decreases with each subsequent CV cycle until the voltammogram returns to that characteristic for Au cycled in Fe-free electrolyte (Figure 3). XPS of the electrodes after cycling in the “Fe-free” electrolyte shows no signals corresponding to Fe.

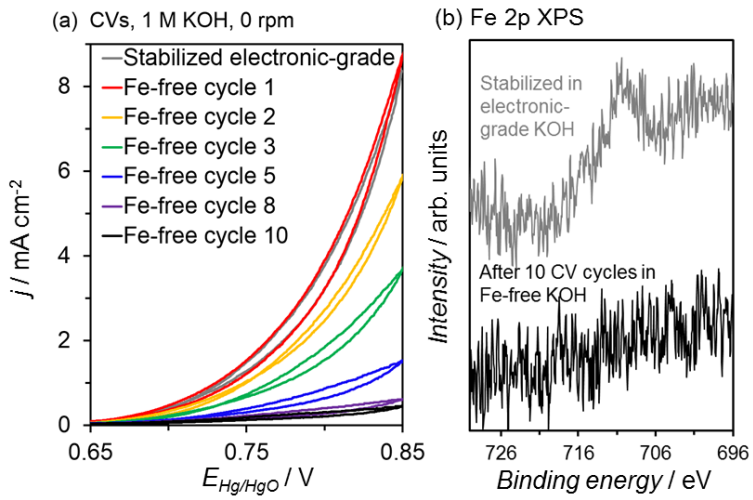

Figure 3. Cyclic voltammetry (a) and photoelectron spectra (b) of Au electrodes after initial cycling from 0.0 to 0.85 V in electronic-grade 1 M KOH (gray) and after subsequent transfer and cycling in "Fe-free" 1 M KOH (black). E^0 for OER is 0.306 V vs. Hg/HgO, and the scan rate is 10 mV s^{-1}. Raw XPS data were smoothed using 3-point adjacent averaging.

To investigate the stability of Fe over Au at OER current densities of practical interest (~10 mA cm^{-2}), voltammograms were acquired with higher anodic scan limits (0.9-1.1 V). An oxidation feature is clearly observed above 0.8 V vs Hg/HgO in reagent-grade KOH (Figure 4b) for CV scans carried out to higher anodic potentials, but this feature is absent in purified ("Fe-free") KOH electrolyte (Figure 6a). After immersing a Au electrode overnight in 1 M reagent-grade KOH with no applied potential, a similar anodic peak is observed during the first CV cycle (Figure 4c). Based upon the difference between the CVs of Figures 4a and 4b, we hypothesize that the observed oxidation wave is related to the presence (and oxidation) of Fe surface species, and from the results shown in Figure 4c, that these surface species can accumulate spontaneously in the absence of applied potential.

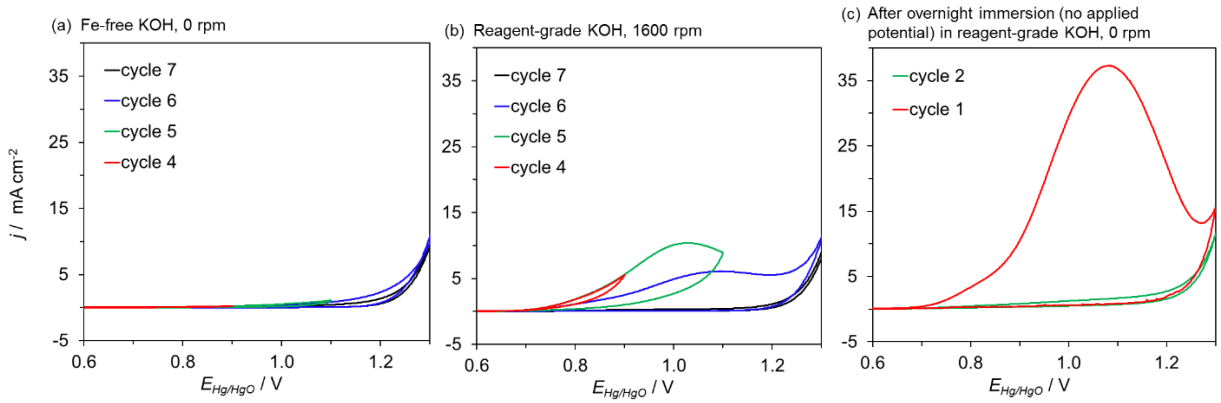

Figure 4. Cyclic voltammograms of Au cycled in (a) "Fe-free" 1 M KOH and (b) reagent-grade 1 M KOH, both after three cycles of stabilization cycling to 0.8 V, and (c) after overnight immersion (with no applied potential) in reagent-grade 1 M KOH. The potential was scanned at a rate of 10 mV s^{-1} between 0 and 0.9-1.3 V vs Hg/HgO, for which E^0 for the OER is 0.306 V.

The results presented above clearly demonstrate that the interaction of Fe^{3+}cations with the surface of the Au electrode is reversible. This then raises the question of how such cations react with the surface and are removed from it. We begin by noting that the surface of Au immersed in 1 M KOH contains a mixture of hydroxide and oxide species, depending on the applied potential: spectroscopic evidence shows that hydroxide anions will adsorb specifically on Au at potentials below 0.3 V vs Hg/HgO in 0.1 M KOH, and that a mixture of Au oxide/hydroxide is formed at potentials above about 0.3 V.[5a, 12] In alkaline pH, soluble Fe^{3+} species are expected to be present as FeO_2^- anions.[13] Since the accumulation of surface Fe occurs in the absence of an applied potential, we hypothesize that the following reaction may occur:

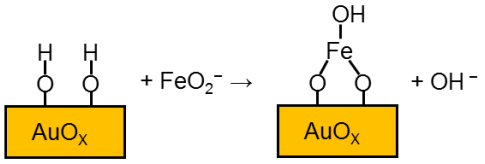

(1)

In this simplified representation (for a more detailed structure, see the next section), x = 0.0-1.5 in AuO_x, depending on the extent of oxidation of the Au surface.

We hypothesize further that the oxidation wave observed in Figures 4b and 4c is attributable to oxygen evolution coupled with the electrochemical oxidation of surface Fe^{3+} to ferrate(VI) anions via the following reaction:

. (2)

Reaction 2 is identical to that proposed to occur on Fe electrodes[14] and on a Pt electrode immersed in a solution containing 0.007 M FeO_2^- [15] (all in highly concentrated, 10-15 M alkaline electrolytes). The oxidation peaks observed in these studies were attributed to the formation of ferrate(VI) ions (FeO_4^{2-}) and occurred at potentials overlapping the onset of oxygen evolution.[15-16] Thus, we propose that the adsorption of Fe^{3+} cations via Reaction 1 occurs at low anodic potentials and that the removal of these cations from the surface occurs as the potential is raised, concurrent with the onset of the OER. Since only a fraction of the Fe initially on the surface is removed in any CV cycle, repeated cycling leads to further removal of the Fe^{3+}cations and the loss in OER activity seen in Figures 4b and 4c.

Reactions 1 and 2 can also be used to explain the experimental observations of Doyle and Lyons for Au in 1 M NaOH. These authors (and others) observe an oxidation peak at η = 0.4-0.9 V after CV cycling from -0.8 to 0.8 V vs RHE (or -1.7 to -0.1 V vs Hg/HgO at pH 14),[3-4] which they attribute to oxygen evolution over a transient, catalytically active Au(III) surfaquo species. Using a rotating-ring disc, they detected an oxygen reduction current on the ring electrode for η = 0.4-0.9 V, confirming that the current generated at the working electrode disc during the oxidation wave is due (at least in part) to oxygen evolution.[3] Since the surface Fe^{3+} species we propose are also expected to be the catalytically-active sites for oxygen evolution at these potentials, it is not possible to separate the current contributions due to the oxygen evolution reaction from those due to the formation of ferrate(VI) species, but it is clear that both processes occur in the same potential range. A plateau or decrease in current is observed with subsequent anodic potential scans because ferrate(VI) species are soluble and hence their formation results in the removal Fe from the electrode surface via Reaction 2, thereby lowering the number of active sites for OER and the OER contribution to the measured current.

Doyle and Lyons also noted the occurrence of two reduction waves (termed C2' and C2") on "activated" Au,[3] which they suggested are due to the reduction of different forms of hydrous oxides. In the presence of Fe impurities, we observe similar reduction features in the same potential window, from 0.0 to -0.5 V vs Hg/HgO (Figure 5). We note that the potentials at which these features appear coincide closely with the potentials at which ferrate(VI) reduction (Reaction 3) has been reported to occur.[13-15, 17]

$$FeO_4^{2-} + 2H_2O + 3e^- \rightarrow FeO_2^- + 4OH^- \quad (3)$$

Oxygen reduction is also expected to occur below ~0.0 V vs Hg/HgO. An increase in the magnitude of these reduction features with additional activation cycling (as observed by Doyle and Lyons) would be consistent with the accumulation of Fe impurities on the Au surface via Reaction 1. With the subsequent anodic scan, a larger number of ferrate(VI) species would be formed, and during the return (cathodic) sweep, a greater reduction current due to Reaction 3 would be expected. We note that the ferrate reduction features are smaller than the oxidation wave above 0.7 V due to the removal of surface Fe via Reaction 2. This is likely due to 1) diffusion of the ferrate FeO_4^{2-} anions away from the electrode surface and 2) slow chemical decomposition of ferrate(VI) anions via the reaction $FeO_4^{2-} + 1/2H_2O \rightarrow FeO_2^- + O_2 + OH^-$. This decomposition has been observed after ~30 min in 5 M KOH.[13, 18] Therefore, we expect the electrochemical conversion of FeO_4^{2-} to FeO_2^- to predominate on the timescale of the CV experiments conducted in the present study.

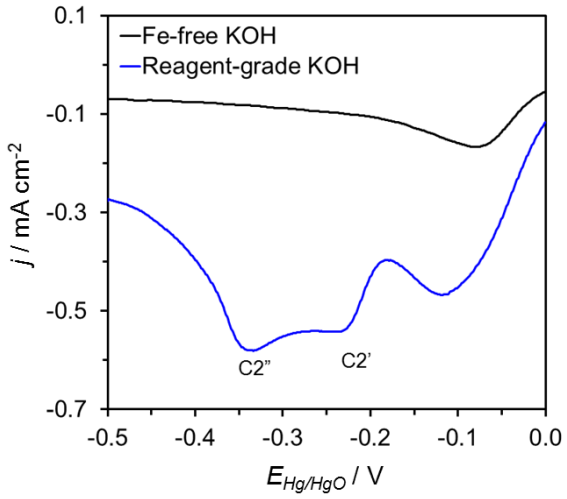

Figure 5. Cathodic scans of Au cycled in "Fe-free" and reagent-grade 1 M KOH. The potential was scanned at a rate of 10 mV s^{-1} after 10 cycles between 0 and 0.8 V vs Hg/HgO, for which E^0 for the OER is 0.306 V.

In summary, we attribute the oxidation and reduction waves ascribed previously[3] to the formation of a highly-active Au(III) surfaquo species and hydrous oxide reduction, respectively, to the formation and reduction of ferrate(VI) species in unpurified alkaline electrolytes. The Fe^{3+} electrolyte impurities (present as FeO_2^- in solution) can chemically bind to the Au oxide/hydroxide surface, even in the absence of an applied potential. These species appear to be significantly more catalytically active than pure Au_2O_3, but at overpotentials of 0.4-0.9 V, the surface-bound Fe^{3+} species are oxidized to ferrate(VI) and removed from the hydroxyl-terminated Au_2O_3 surface.

3.3 Theoretical analysis of oxygen evolution activity of Fe-Au_2O_3

DFT calculations (for complete computational details, see SI, S5) were carried out in order to obtain further insights into the cause for the decrease in the OER overpotental observed when Fe is chemically bound to the surface of Au_2O_3. Previous investigations have shown that under conditions relevant to oxygen evolution, Au is oxidized to Au_2O_3.[6c] To establish the most appropriate surface structure to use in the model of oxygen evolution, several Au_2O_3 surface indices were investigated. Surface energy profiles as a function of the applied potential for the most stable surfaces are shown in Figure 6. At relevant experimental potentials (> 1.23 V vs SHE), the [010] OH-terminated, non-stoichiometric surface (i.e., the surface with the largest surface O/Au ratio relative to that for the bulk O/Au = 1.5) is found to be the most thermodynamically stable, and was chosen therefore for investigation of the energetics of the OER process.

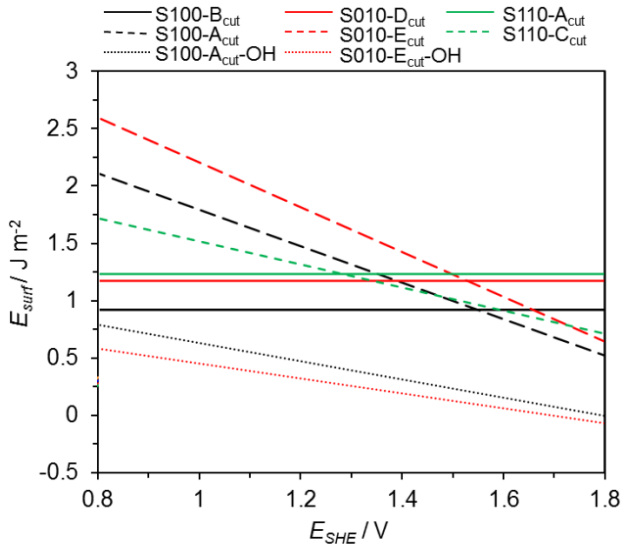

Figure 6. Effect of applied potential on the calculated surface free energies for the [100], [010], and [110] surfaces of Au_2O_3. All possible terminations were considered; however, only the stoichiometric surfaces (S100-B_{cut}, S010-D_{cut}, and S110-A_{cut}) and the most stable non-stoichiometric oxygen-terminated surfaces (S100-A_{cut}, S010-E_{cut}, and S110-C_{cut}) and OH-terminated surfaces (S100-A_{cut}-OH and S010-E_{cut}-OH) are shown. The most stable surface at OER-relevant potentials (> 1.23 V) is the S010-E_{cut}-OH surface, which is used to predict η^{OER}.

The theoretical overpotential calculated from the Gibbs free energy differences between each reaction step is independent of pH, and for greater convenience, can be modeled as if the reaction occurs in an acidic electrolyte:[2d, 8-10, 19]

$$H_2O^* \rightarrow OH^* + e^- + H^+ \quad (4)$$

$$OH^* \rightarrow O^* + e^- + H^+ \quad (5)$$

$$O^* + H_2O \rightarrow OOH^* + e^- + H^+ \quad (6)$$

$$OOH^* \rightarrow O_2 + e^- + H^+ \quad (7)$$

Here * represents a surface vacancy site. The calculated standard hydrogen electrode[9] was used to express the chemical potential of protons and electrons at pH 14 and applied potential *U*.

A schematic of the OER surface intermediates involved in Reactions 4-7 is shown in Figure 7 for both pure Au_2O_3 (top) and Fe-Au_2O_3 (bottom). Table 2 compares the theoretical OER overpotentials to those measured experimentally at a current density of 0.1 mA cm^{-2}

(chosen to avoid potentials where Fe removal from the Au surface is observed in reagent-grade 1 M KOH. Corresponding chronopotentiometry data is shown in SI, S6). Consistent with electrochemical experiments, we find by DFT that the substitution of a Au site by Fe reduces η^{OER} by 0.29 V (from 0.82 to 0.53 V). For Fe-free Au_2O_3, the *O intermediate is high in energy, and the potential determining step is therefore Reaction 5 (*OH oxidation to *O), while for Fe-Au_2O_3, the *O intermediate is relatively more stable and the potential determining step is Reaction 6 (*O oxidation to *OOH). These changes can be explained as follows: because the *d*-orbitals of Au are nearly filled and are unable to form π-bonds with oxygen, Au sites bind oxo species very weakly, whereas Fe has fewer *d*-electrons and can form π-bonds with oxygen, leading to more stable Fe=O structures.[20] Consequently, the binding energetics of OER reaction intermediates attached to Fe cations bound to the surface of Au_2O_3 are more optimal than those of intermediates attached to Au cations.

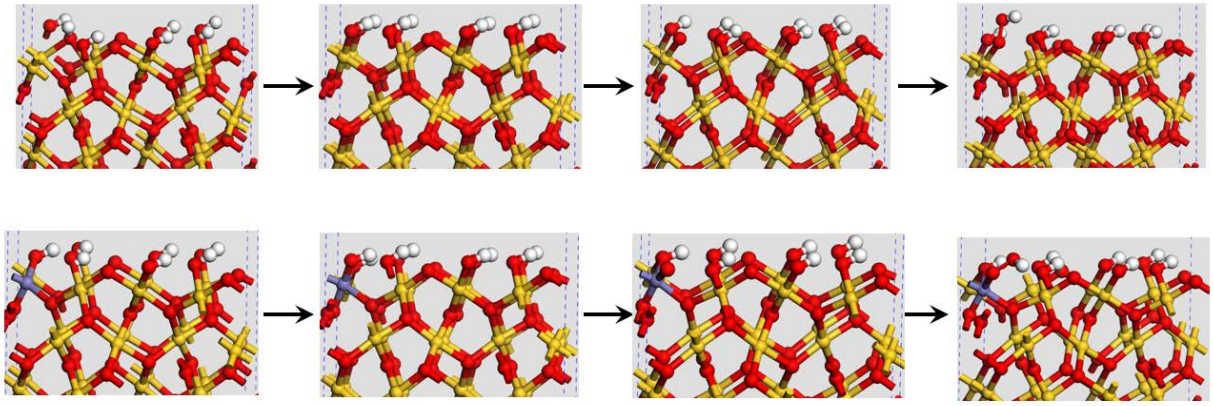

Figure 7. Structures of the intermediates (Reactions 4-7) of the OER over pure Au_2O_3 (top) and Fe chemically bound to Au_2O_3 (bottom). Au atoms are shown in gold and Fe atoms are shown in blue.

Table 2. Comparison of experimental and computational OER overpotentials

	Experimental η (j = 0.1 mA cm^{-2}) (V)	Computational η (V)
Au_2O_3	0.84	0.82
Fe-Au_2O_3	0.49	0.53

4. Conclusions

Fe cations present as impurities in 1 M KOH react with the surface of Au electrodes and create active centers for the OER. An increase in the current density above the onset potential for the OER correlates with the accumulation of Fe at the electrode surface. The OER overpotential over Au decreases from ~0.85 to ~0.4 V with the presence of surface Fe sites at low current densities ($j = 0.1$ mA cm^{-2}), in close agreement with the decrease in the OER overpotential determined from DFT calculations for pure Au_2O_3 vs Fe chemically bound to Au_2O_3. This decrease in the OER overpotential is attributed to the more optimal adsorption energy of intermediates involved in the oxygen evolution reaction. The nearly-filled d-orbitals of Au cause the adsorbed oxo species present on the surface of Au_2O_3 to be weakly bound, while the less occupied d-orbitals of Fe can bind these oxo species more strongly. In contrast to what has been observed for CoOOH and NiOOH, chemical binding of Fe to Au oxide is reversible at the potentials of interest, and the removal of surface Fe coincides with an oxidation wave at 0.7-1.2 V vs Hg/HgO ($\eta = 0.4$-0.9 V). With increased current densities, the applied overpotential reaches a level where Fe removal occurs via the formation of aqueous ferrate(VI) species.

ACKNOWLEDGEMENTS

This material is based upon work performed by the Joint Center for Artificial Photosynthesis, a DOE Energy Innovation Hub, supported through the Office of Science of the U.S. Department of Energy under Award Number DE-SC0004993. The authors gratefully acknowledge James Wu and Doug Jamieson (Lawrence Berkeley National Laboratory) for RDE fabrication. The authors also thank Li Wang (Lawrence Berkeley National Laboratory) for ICP-MS acquisition, as well as Jason Cooper and David Larson (Joint Center for Artificial Photosynthesis) for assistance with the acquisition of XPS data.

TOC graphic:

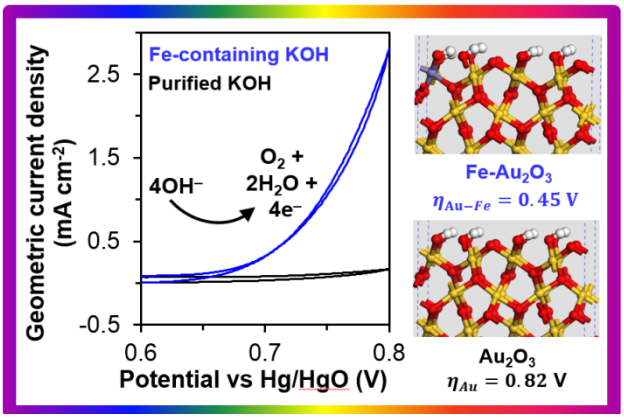
Fe-containing KOH
Purified KOH
Geometric current density (mA cm-2)
2.5
1.5
0.5
-0.5
0.6
0.7
0.8
Potential vs Hg/HgO (V)
4OH−
O2 + 2H2O + 4e−
Fe-Au2O3
ηAu−Fe = 0.45 V
Au2O3
ηAu = 0.82 V

References

[1] aI. Katsounaros, S. Cherevko, A. R. Zeradjanin, K. J. J. Mayrhofer, *Angewandte Chemie-International Edition* **2014**, *53*, 102-121; bN. S. Lewis, D. G. Nocera, *Proceedings of the National Academy of Sciences of the United States of America* **2006**, *103*, 15729-15735; cD. Gust, T. A. Moore, A. L. Moore, *Accounts of Chemical Research* **2009**, *42*, 1890-1898; dZ. G. Yang, J. L. Zhang, M. C. W. Kintner-Meyer, X. C. Lu, D. W. Choi, J. P. Lemmon, J. Liu, *Chemical Reviews* **2011**, *111*, 3577-3613; eM. G. Walter, E. L. Warren, J. R. McKone, S. W. Boettcher, Q. Mi, E. A. Santori, N. S. Lewis, *Chemical Reviews* **2010**, *110*, 6446-6473; fT. R. Cook, D. K. Dogutan, S. Y. Reece, Y. Surendranath, T. S. Teets, D. G. Nocera, *Chemical Reviews* **2010**, *110*, 6474-6502; gJ. R. McKone, N. S. Lewis, H. B. Gray, *Chemistry of Materials* **2014**, *26*, 407-414; hD. Pletcher, X. Li, *International Journal of Hydrogen Energy* **2011**, *36*, 15089-15104; iA. Singh, L. Spiccia, *Coordination Chemistry Reviews* **2013**, *257*, 2607-2622; jJ. Suntivich, K. J. May, H. A. Gasteiger, J. B. Goodenough, Y. Shao-Horn, *Science* **2011**, *334*, 1383-1385.

[2] aM. S. Burke, M. G. Kast, L. Trotochaud, A. M. Smith, S. W. Boettcher, *Journal of the American Chemical Society* **2015**, *137*, 3638-3648; bS. Klaus, Y. Cai, M. W. Louie, L. Trotochaud, A. T. Bell, *The Journal of Physical Chemistry C* **2015**, *119*, 7243-7254; cL. Trotochaud, S. L. Young, J. K. Ranney, S. W. Boettcher, *Journal of the American Chemical Society* **2014**, *136*, 6744-6753; dD. Friebel, M. W. Louie, M. Bajdich, K. E. Sanwald, Y. Cai, A. M. Wise, M.-J. Cheng, D. Sokaras, T.-C. Weng, R. Alonso-Mori, R. C. Davis, J. R. Bargar, J. K. Nørskov, A. Nilsson, A. T. Bell, *Journal of the American Chemical Society* **2015**, *137*, 1305-1313; eM. W. Louie, A. T. Bell, *Journal of the American Chemical Society* **2013**, *135*, 12329-12337; fC. Iwakura, A. Honji, H. Tamura, *Electrochimica Acta* **1981**, *26*, 1319-1326; gE. Laouini, M. Hamdani, M. I. S. Pereira, J. Douch, M. H. Mendonça, Y. Berghoute, R. N. Singh, *International Journal of Hydrogen Energy* **2008**, *33*, 4936-4944; hT. Grewe, X. Deng, H. Tüysüz, *Chemistry of Materials* **2014**, *26*, 3162-3168; iC. C. L. McCrory, S. Jung, J. C. Peters, T. F. Jaramillo, *Journal of the American Chemical Society* **2013**, *135*, 16977-16987; jK. J. May, C. E. Carlton, K. A. Stoerzinger, M. Risch, J. Suntivich, Y.-L. Lee, A. Grimaud, Y. Shao-Horn, *The Journal of Physical Chemistry Letters* **2012**, *3*, 3264-3270; kD. A. Corrigan, *Journal of The Electrochemical Society* **1987**, *134*, 377-384.

[3] R. Doyle, M. G. Lyons, *J Solid State Electrochem* **2014**, *18*, 3271-3286.

[4] L. D. Burke, V. J. Cunnane, B. H. Lee, *Journal of the Electrochemical Society* **1992**, *139*, 399-406.

[5] aB. S. Yeo, S. L. Klaus, P. N. Ross, R. A. Mathies, A. T. Bell, *ChemPhysChem* **2010**, *11*, 1854-1857; bP. E. Karthik, C. Jeyabharathi, K. L. Phani, *Chemical Communications* **2014**, *50*, 2787-2790; cS. Cherevko, A. R. Zeradjanin, G. P. Keeley, K. J. J. Mayrhofer, *Journal of the Electrochemical Society* **2014**, *161*, H822-H830; dT. T. H. Hoang, Y. Cohen, A. A. Gewirth, *Analytical Chemistry* **2014**, *86*, 11290-11297; eS. H. Othman, M. S. El-Deab, T. Ohsaka, *International Journal of Electrochemical Science* **2011**, *6*, 6209-6219.

[6] aM. Peuckert, F. P. Coenen, H. P. Bonzel, *Surf. Sci.* **1984**, *141*, 515-532; bK. Juodkazis, J. Juodkazyte, V. Jasulaitiene, A. Lukinskas, B. Sebeka, *Electrochem. Commun.* **2000**, *2*, 503-507; cO. Diaz-Morales, F. Calle-Vallejo, C. de Munck, M. T. M. Koper, *Chemical Science* **2013**, *4*, 2334-2343.

[7] NIST X-ray Photoelectron Spectroscopy Database, Version 4.1, **2012**.

[8] J. Rossmeisl, Z. W. Qu, H. Zhu, G. J. Kroes, J. K. Nørskov, *Journal of Electroanalytical Chemistry* **2007**, *607*, 83-89.
[9] J. K. Nørskov, J. Rossmeisl, A. Logadottir, L. Lindqvist, J. R. Kitchin, T. Bligaard, H. Jónsson, *The Journal of Physical Chemistry B* **2004**, *108*, 17886-17892.
[10] J. Rossmeisl, A. Logadottir, J. K. Nørskov, *Chemical Physics* **2005**, *319*, 178-184.
[11] aV. Tripković, E. Skúlason, S. Siahrostami, J. K. Nørskov, J. Rossmeisl, *Electrochimica Acta* **2010**, *55*, 7975-7981; bM. J. Janik, C. D. Taylor, M. Neurock, *Journal of The Electrochemical Society* **2009**, *156*, B126-B135; cJ. Sun, Y.-H. Fang, Z.-P. Liu, *Physical Chemistry Chemical Physics* **2014**, *16*, 13733-13740.
[12] aJ. Desilvestro, M. J. Weaver, *Journal of Electroanalytical Chemistry and Interfacial Electrochemistry* **1986**, *209*, 377-386; bY. Zhang, X. Gao, M. J. Weaver, *The Journal of Physical Chemistry* **1993**, *97*, 8656-8663.
[13] F. Beck, R. Kaus, M. Oberst, *Electrochimica Acta* **1985**, *30*, 173-183.
[14] aM. De Koninck, D. Bélanger, *Electrochimica Acta* **2003**, *48*, 1435-1442; bZ. Mácová, K. Bouzek, V. Sharma, *J Appl Electrochem* **2010**, *40*, 1019-1028.
[15] K. Bouzek, I. Roušar, H. Bergmann, K. Hertwig, *Journal of Electroanalytical Chemistry* **1997**, *425*, 125-137.
[16] J. Híveš, Z. Mácová, M. Benová, K. Bouzek, *Journal of The Electrochemical Society* **2008**, *155*, E113-E119.
[17] A. S. Venkatadri, W. F. Wagner, H. H. Bauer, *Analytical Chemistry* **1971**, *43*, 1115-1119.
[18] W. F. Wagner, J. R. Gump, E. N. Hart, *Analytical Chemistry* **1952**, *24*, 1497-1498.
[19] I. C. Man, H.-Y. Su, F. Calle-Vallejo, H. A. Hansen, J. I. Martínez, N. G. Inoglu, J. Kitchin, T. F. Jaramillo, J. K. Nørskov, J. Rossmeisl, *ChemCatChem* **2011**, *3*, 1159-1165.
[20] K. P. O'Halloran, C. Zhao, N. S. Ando, A. J. Schultz, T. F. Koetzle, P. M. B. Piccoli, B. Hedman, K. O. Hodgson, E. Bobyr, M. L. Kirk, S. Knottenbelt, E. C. Depperman, B. Stein, T. M. Anderson, R. Cao, Y. V. Geletii, K. I. Hardcastle, D. G. Musaev, W. A. Neiwert, X. Fang, K. Morokuma, S. Wu, P. Kögerler, C. L. Hill, *Inorganic Chemistry* **2012**, *51*, 7025-7031.